**Science and Technology Indonesia**
*e*-ISSN:2580-4391 *p*-ISSN:2580-4405
Vol. 11, No. 2, April 2026

Research Paper

# Microwave-Assisted Cocrystallization of *p*-Methoxycinnamic Acid with Saccharin and Nicotinamide: Comparative Effects on Solubility and Dissolution

Abhimata Paramanandana[1,2*], Kurnia Kawaguchi[1,2], Melanny Ika Sulistyowaty[1,3], Marey Almaghrabi[4], Dwi Setyawan[1,2]

[1]*Department of Pharmaceutical Sciences, Faculty of Pharmacy, Universitas Airlangga, Campus C UNAIR Mulyorejo, Surabaya, 60115, Indonesia*
[2]*Pharmaceutics and Delivery Systems for Drugs, Cosmetic, and Nanomedicine Research Group, Faculty of Pharmacy, Universitas Airlangga, Campus C UNAIR Mulyorejo, Surabaya, 60115, Indonesia*
[3]*Drug Development Research Group, Faculty of Pharmacy, Universitas Airlangga, Campus C UNAIR Mulyorejo, Surabaya, 60115, Indonesia*
[4]*Department of Pharmaceutics and Industrial Pharmacy, Faculty of Pharmacy, Taibah University, Madinah, 42353, Saudi Arabia*
*__Corresponding author__: abhimata.p@ff.unair.ac.id

**Abstract**
*p*-methoxycinnamic acid (*p*MCA) has activity as an anti- inflammatory and analgesic but is difficult to dissolve in water with a solubility of only 0.712 mg/mL at 25 °C. Poor solubility will result a low dissolution rate so that drug absorption becomes limited, affects the bioavailability, and causes therapeutic effect to become less optimal. The formation of co-crystals are able to improve the solubility properties and dissolution rate by physically modifying the active compound. Cocrystals are crystalline materials composed of two or more molecules at specific stoichiometric ratios to form non-covalent bonds. Both saccharin and nicotinamide can be use as coformers because saccharin and nicotinamide were able to increase the solubility and dissolution rate of active compounds due to the formation of non-covalent bonds. The results showed that the formation of cocrystals using the microwave radiation had a higher solubility and dissolution rate of *p*MCA compared to pure *p*MCA. The *p*MCA-nicotinamide cocrystal increased solubility 1.29 times higher than a single *p*MCA while the *p*MCA-saccharin cocrystal increased solubility only 1.26 times higher than a single *p*MCA. In the dissolution rate test, the *p*MCA-Nicotinamide cocrystal increased the dissolution rate 3.67 times higher while the *p*MCA-Saccharin only increased 3.55 times higher than a single *p*MCA. These results show that both cocrystals have better solubility and dissolution rate properties than pure *p*MCA so it can be said that forming cocrystals can increase the solubility and dissolution rate of *p*MCA. Based on this study findings, it can also confirm that formation cocrystal *p*MCA using nicotinamide coformers has a good solubility and dissolution rate than formation cocrystal using saccharin coformers.

**Keywords**
*p*-Methoxycinnamic Acid, Nicotinamide, Saccharin, Cocrystal, Microwave Radiation, Dissolution

Received: 29 October 2025, Accepted: 16 January 2026
https://doi.org/10.26554/sti.2026.11.2.436-446

## 1. INTRODUCTION

Solubility is a critical parameter in oral drug development, as it directly affects dissolution, absorption, and therapeutic efficacy (Palanisamy and Khanam, 2011; Tambosi et al., 2018). Poor aqueous solubility remains a major challenge, limiting bioavailability and resulting in limited therapeutic outcomes. It is estimated that more than 40% of marketed drugs are poorly soluble in water (Nyamba et al., 2024), including *p*-methoxycinnamic acid (*p*MCA). *p*MCA is a cinnamic acid derivative found predominantly in the rhizomes of *Kaempferia galanga* L. (kencur) (Subositi et al., 2020). *p*MCA has various pharmacological fucntion, including analgesic, anti-inflammatory, and antihyperglycemic effects (Adisakwattana et al., 2005; Ekowati and Diyah, 2013), but its low solubility (0.712 mg/mL at 25 °C) restricts oral bioavailability.

Several strategies have been developed to improve drug solubility, including reducing particle size, polymorphism, amorphization, solid dispersions, and chemical modifications such as salt or complex formation (Savjani et al., 2012). Among these, cocrystallization has become one of the promising approach because it can improve solubility, dissolution, bioavailability, and stability without altering the pharmacological activity of the API (Bavishi and Borkhataria, 2016; Sathisaran and Dalvi, 2018). Cocrystals are crystalline materials formed by an API and a coformer through non-covalent interactions such as hydrogen bonding or $\pi$-$\pi$ stacking (Miroshnyk et al., 2009). Cocrystals main mechanism improving solubility is by reducing the API crystal lattice energy and exposing the hydrophilic structure of the coformers by reducing steric hinderance (Setyawan et al., 2025). Therefore, the choice of coformer

is crucial for successful cocrystallization. Saccharin and nicotinamide are well-established, safe pharmaceutical excipients whose functional groups readily participate in hydrogen bonding, making them suitable coformers for cocrystal formation (Karagianni et al., 2018; Setyawan et al., 2014). Numerous studies have demonstrated that these coformers significantly enhance drug solubility, dissolution, stability, and permeability, as observed in enzalutamide-saccharin (Prashanth et al., 2022), indomethacin-saccharin (Basavoju et al., 2008), quercetin-nicotinamide (Dias et al., 2022), and cefixime-nicotinamide cocrystals (Abdullah et al., 2022). Furthermore, their ability to form stable hydrogen-bonded networks is supported by both structural evidence (Prashanth et al., 2022) and $pK_a$ considerations, with $\Delta pK_a$ values for *p*MCA-saccharin ($\Delta pK_a$ = 2.287) and *p*MCA-nicotinamide ($\Delta pK_a$ = 0.537) falling within the range favorable for cocrystal formation (Qiao et al., 2011). Collectively, these findings validate the selection of saccharin and nicotinamide as effective and rational coformers for improving the physicochemical properties of poorly soluble drugs.

Various methods can be employed to produce pharmaceutical cocrystals, including solvent evaporation, grinding, and supercritical fluid technology. Microwave-assisted crystallization has recently gained attention as a green chemistry technique due to its rapid, selective heating, reduced processing time, and environmental compatibility (Gillespie, 2005; Pagire et al., 2013). Additionally, this approach minimizes environmental impact and improves process efficiency (Ahmad et al., 2024). Nevertheless, there is still a large gap in the use of microwave-assisted synthesis for this objective. The majority of published research concentrates on traditional synthesis techniques or exclusively examines microwave-assisted synthesis in broad chemical contexts, with little attention paid to its application in drug cocrystal production (Puspita et al., 2025). This unexplored field offers a chance to improve microwave assisted synthesis in pharmaceutical formulation both practically and scientifically.

Although producing cocrystals have been widely reported Sulistyowaty et al. (2024), studies employing microwave irradiation for their preparation are limited. Therefore, the novelty of this work lies in the application of an environmentally friendly microwave-assisted method for the preparation of *p*MCA cocrystals which not only addresses the existing research gap but also offers a practical and sustainable alternative for pharmaceutical cocrystal fabrication, contributing to both scientific understanding and formulation development. this study aimed to enhance the solubility and dissolution of *p*MCA by forming cocrystals with saccharin and nicotinamide at a 1:1 molar ratio using microwave radiation. The prepared solids were characterized using X-ray diffraction (XRD), differential scanning calorimetry (DSC), Fourier-transform infrared spectroscopy (FTIR), and scanning electron microscopy (SEM). Solubility and dissolution studies were conducted to evaluate the extent of improvement compared to pure *p*MCA and its physical mixtures.

## 2. EXPERIMENTAL SECTION

### 2.1 Material

*p*-Methoxycinnamate acid were obtained from Himedia Laboratories Pvt., Ltd., India, (Lot :0000520525) and saccharine were purchased from Sigma Aldrich, USA (Lot: MKBJ0082V). Nicotinamide, sodium hydroxide (NaOH), Ethanol 96% Pro analysis, $NaH_2PO_4.H_2O$ and $Na_2HPO_4.2H_2O$ were obtained from Merck, Germany and 99.9% indium DSC calibrator were purchased from Linseis, Germany.

### 2.2 Instruments

The instrument used in this study include microwave model R-728(W)-IN (Sharp, Japan) equipped with 900 watt power micro output, Fourier Transform Infrared Spectroscopy (Jasco, USA), Differential Scanning Calorimeter (Linseis, Germany), Scanning Electron Microscope Thermoscientific Phenom ProX (Thermoscientific, USA), Powder X-ray Diffractometer Rigaku® type Miniflex 600C (Rigaku, Japan), and Erweka®DT 700 Dissolution Tester Apparatus 2 (Erweka, Germany).

### 2.3 Methods

#### 2.3.1 Preparation of Physical Mixtures

Physical mixtures of *p*MCA-nicotinamide (PM-PN) and *p*MCA-saccharin (PM-PS) were prepared at a 1:1 molar ratio. Each component was sieved through an 80-mesh sieve (Retsch Type ASTM,USA), accurately weighed, and blended in a mortar using a stainless-steel spatula until a homogeneous mixture was obtained (Sulistyowaty et al., 2024). Specifically, 0.5933 g of *p*MCA was combined with 0.4067 g of nicotinamide, while 0.4931 g of *p*MCA was combined with 0.5069 g of saccharin.

#### 2.3.2 Preparation of Cocrystals by Microwave Radiation

Nicotinamide and saccharin were selected as distinct coformers and combined with *p*MCA in a 1:1 molar ratio to prepare *p*MCA cocrystals. The preparation method was adapted with slight modifications from procedures reported by Sulistyowaty et al. (2024) and Setyawan et al. (2025). Accurately weighed *p*MCA and the respective coformers (in amounts equivalent to those used for physical mixtures) were mixed, moistened with 10% (w/w) distilled water, and exposed to microwave model R-728(W)-IN (Sharp, Japan) with a continuous irradiation at 450 W for 15 minutes. To avoid residual heat interference, the microwave oven was left unused for at least 5 hours prior to the experiment. The resulting *p*MCA-nicotinamide (CC-PN) and *p*MCA-saccharin (CC-PS) cocrystals were collected, dried in a desiccator for 48 hours, and sieved through an 80-mesh sieve before further analysis. The yields obtained for CC-PN and CC-PS were 98.81 ± 0.29% and 101.11 ± 0.46%, respectively, based on triplicate preparations.

#### 2.3.3 Fourier Transform Infrared Spectroscopy (FTIR Spectroscopy)

Infrared spectra were obtained using an FTIR spectrometer (Jasco, USA) equipped with an ATR crystal plate accessory. Approximately 0.05 g of each sample was placed on the crystal

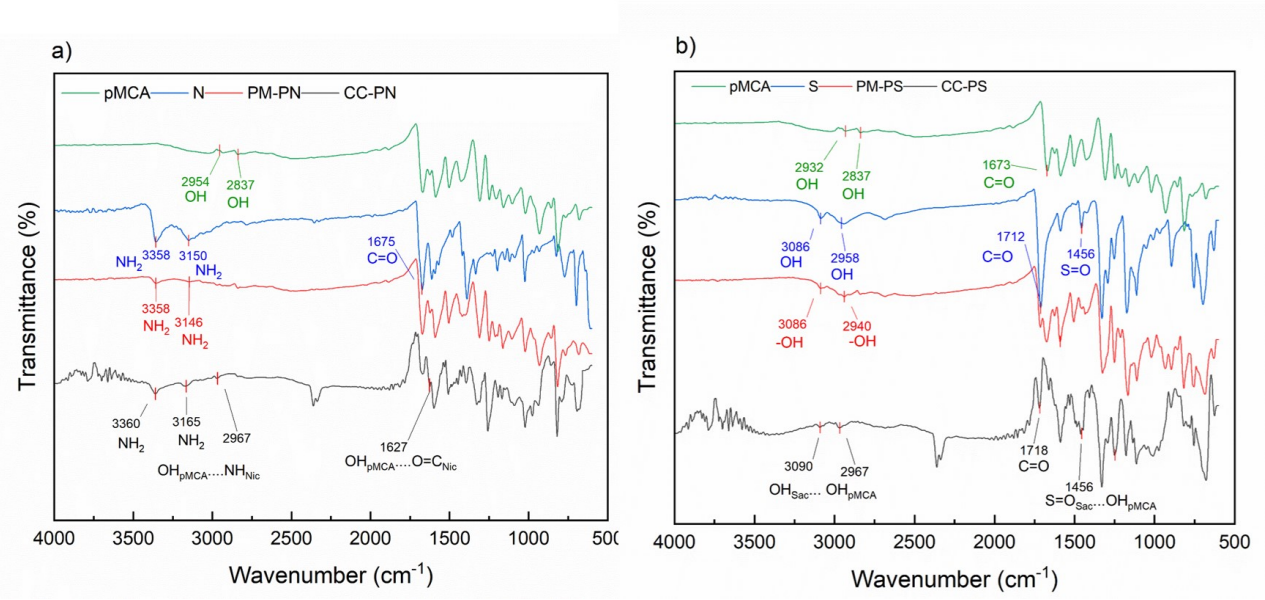


**Figure 1.** FTIR Spectra of (a) *p*MCA (Green), Nicotinamide (Blue), Physical Mixture PM-PN (Red), and Cocrystal CC-PN (Black); and (b) *p*MCA (Green), Saccharin (Blue), Physical Mixture PM-PS (Red), and Cocrystal CC-PS (Black)

surface and allowed to stabilize for 3 minutes before scanning. Spectral data were recorded across 4000-500 $cm^{-1}$ and compared against the spectra of the individual raw materials (Setyawan et al., 2018).

### 2.3.4 Thermal Analysis

Thermal profiles were determined using a Differential Scanning Calorimetry (DSC) (Linseis, Germany). The instrument was calibrated with 99.9% indium (Linseis, Germany) prior to analysis. Accurately weighed samples (5-7 mg) were heated at 10 °C/min from 30 °C to 300 °C in a sealed aluminum pans (Setyawan et al., 2020).

### 2.3.5 Surface Morphology

Surface morphologies of *p*MCA, nicotinamide, and saccharin were observed using SEM. approximately 10 mg of each sample was mounted onto aluminum stubs using double-sided carbon adhesive tape, followed by gold coating to a thickness of 5 nm. The coated samples were then observed under the SEM at a magnification of 2000× to evaluate surface morphology, particle characteristics and particle size distribution (Setyawan et al., 2025; Xiao et al., 2022).

**Table 1.** Slope Value Calculated from Dissolution Profiles. Presented Data was the Mean ± SD ($n$=3)

| Sample | Slope |
|---|---|
| *p*MCA | 0.0383 ± 0.0006 |
| PM-PN | 0.1159 ± 0.0004 |
| PM-PS | 0.0587 ± 0.0010 |
| CC-PN | 0.1405 ± 0.0033 |
| CC-PS | 0.0853 ± 0.0006 |

### 2.3.6 Crystallinity

The crystalline patterns of pure *p*MCA, coformers, and prepared systems were analyzed using PXRD. Approximately 100 mg of samples were gently placed and leveled on a sample holder to reduce orientation bias. Diffractograms were collected in the $2\theta$ range of 5-50° with Cu K$\alpha$ radiation at 40 kV and 40 mA (Setyawan et al., 2018).

### 2.3.7 Solubility Studies

Equilibrium solubility was evaluated for pure *p*MCA, physical mixtures, and cocrystals. Samples equivalent to 25 mg of *p*MCA (42.13 mg for *p*MCA-nicotinamide and 50.70 mg for *p*MCA-saccharin) were introduced into 25 mL of phosphate buffer (pH 6.8) and stirred at 600 rpm at 25 ± 0.5 °C. After 5 h, aliquots (5 mL) were withdrawn, filtered through a 0.45 $\mu$m membrane, and diluted (100 $\mu$L into 5 mL buffer). Concentrations were determined using UV-Vis spectrophotometry type UK 5300 (Hitachi, Japan) at the $\lambda$ max of *p*MCA. All experiments were conducted in triplicate (Sulistyowaty et al., 2024).

### 2.3.8 Dissolution Studies

Dissolution behavior was examined using a Erweka Dissoluion tester DT 700 USP type II (paddle) (Erweka, Germany) apparatus containing 900 mL phosphate buffer (pH 6.8) maintained at 37 ± 0.5 °C and stirred at 75 rpm. Samples equivalent to 50 mg *p*MCA were tested: pure *p*MCA (50 mg), *p*MCA-nicotinamide (84.26 mg), and *p*MCA-saccharin (101.40 mg). At predetermined time points (5, 10, 15, 30, 45, and 60 min), 5 mL aliquots were withdrawn and replaced with fresh medium to maintain sink condition. Collected samples were filtered (0.45 $\mu$m) and analyzed by UV-Vis spectrophotometry type

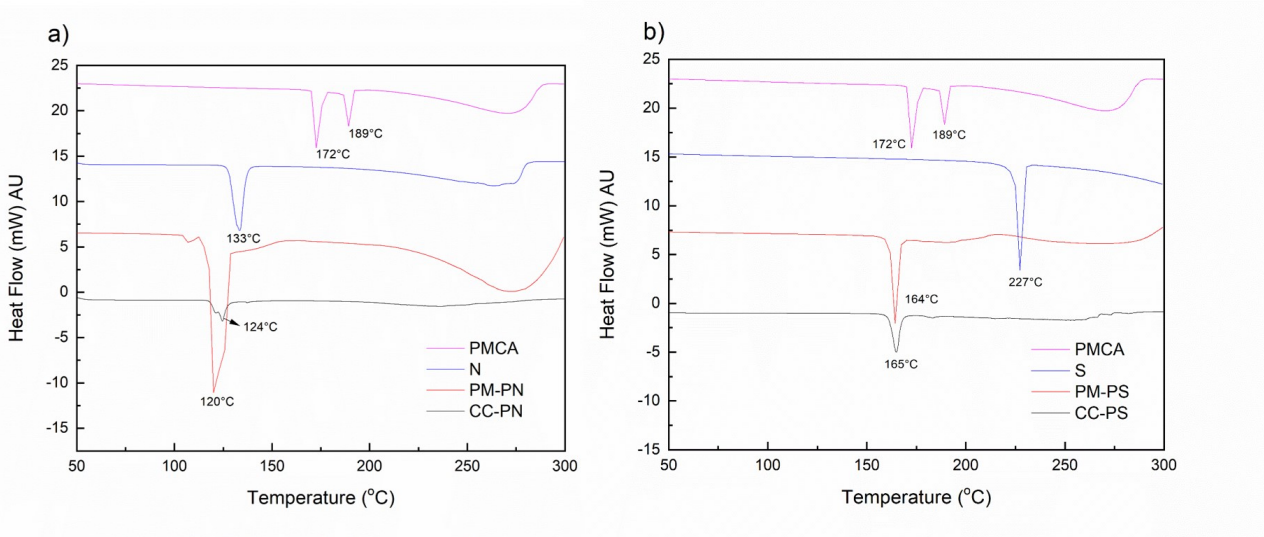


**Figure 2.** DSC Thermograms of (a) *p*MCA (pink), Nicotinamide (Blue), Physical Mixture PM-PN (Red), and Cocrystal CC-PN (Black); and (b) *p*MCA (Pink), Saccharin (Blue), Physical Mixture PM-PS (Red), and Cocrystal CC-PS (Black)

UK 5300 (Hitachi, Japan). Each test was performed in triplicate (Sulistyowaty et al., 2024).

### 2.3.9 Statistical analysis

All solubility data were analyzed using one-way ANOVA at a 95% confidence level ($\alpha$ = 0.05) with SPSS version 26. The one-way ANOVA test was applied to determine whether significant overall differences existed among the treatment groups, with statistical significance defined as $p < 0.05$. A post hoc Least Significant Difference (LSD) test was subsequently performed at the same confidence level ($\alpha$ = 0.05) to identify pairwise differences, where $p < 0.05$ was also considered significant if the ANOVA does not indicate which specific groups differ from each other. Equation 1 was used to obtain the similarity factor ($f_2$), which was used to compare dissolution profile as described by (Ahammad et al., 2015):

$$f_2 = 50 \cdot \log\left\{\left[1 + \frac{1}{n}\sum_{t=1}^{n}(R_t - T_t)^2\right]^{-0.5} \cdot 100\right\} \quad (1)$$

where $n$ is the number of sampling points and $Rt$ and $Tt$ stand for the proportion of dissolved API at each time point for the reference and test formulations, respectively. The analysis utilized data from three-time intervals (5, 10, and 15 minutes). An $f_2$ value below 50 indicated that the dissolution profiles were dissimilar, provided that no more than one time point exceeded 85% drug release, in accordance with international regulatory guidelines (Diaz et al., 2016). To compare dissolution rates among different treatment groups, slope values were calculated based on the Hixson-Crowell cube root law (Sinko and Singh, 2011), which describes the relationship between the cube root of the remaining drug mass and time. This model helps to elucidate the dissolution mechanism associated with surface area changes during the process. The equation is given as follows:

$$M_0^{1/3} - M^{1/3} = k \cdot t \quad (2)$$

where: $M_0$= initial mass of APMS, $M$= mass of undissolved APMS at time, $k$= dissolution rate constant, and $t$ represents time (minutes). The slope obtained from the linear regression of $M_0{}^{1/3}$-$M^{1/3}$ (y-axis) versus time (x-axis) for each treatment group was used to determine and compare the dissolution rates. A higher slope value indicated a faster dissolution rate.

## 3. RESULT AND DISCUSSIONS

### 3.1 Fourier Transform Infrared (FTIR) Analysis

The FTIR spectra conducted to determine possible formation of new intermolecular interactions, indicated by shifts in peak position, intensity, disappearance, or the appearance of new absorption bands. Although the observations were made at wavenumbers between 4000 and 500 $cm^{-1}$ (Figure 1), the confirmation of cocrystal formation was frequently represented as a hydrogen bond at lower wavenumbers (Chaves Júnior et al., 2020). Hydrogen bonding influences vibrational frequencies, enabling identification of the functional groups involved in supramolecular synthon formation (Chadha et al., 2017). In this study, FTIR provided evidence of spectral shifts resulting from interactions between components in the *p*MCA-nicotinamide and *p*MCA-saccharin systems, likely arising from stretching and bending vibrations, which may correlate with the enhanced solubility of the formed cocrystals (Setyawan et al., 2025). *p*MCA exhibits characteristic –OH stretching bands at 2954 and 2837 $cm^{-1}$ and C=C stretching bands at 1587.60 and 1502.75 $cm^{-1}$. Nicotinamide shows $NH_2$ stretching bands at 3358 and 3150 $cm^{-1}$, while saccharin presents –OH stretching

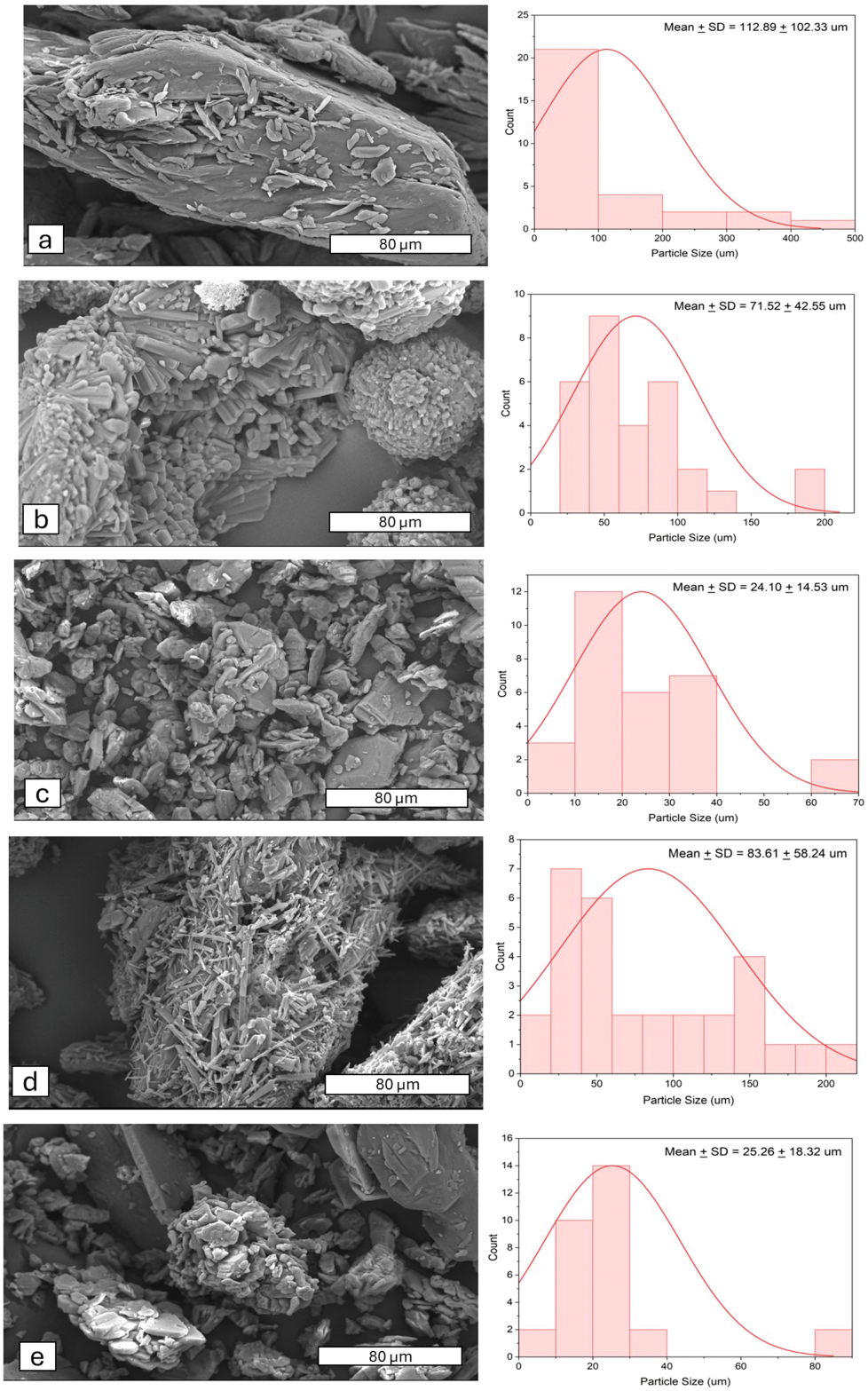


**Figure 3.** SEM Micrographs and Particle Size Distribution of (a) PMCA, (b) Nicotinamide, (c) Saccharin, (d) CC-PN, and (e) CC-PS. Magnification of 2000× Magnifications

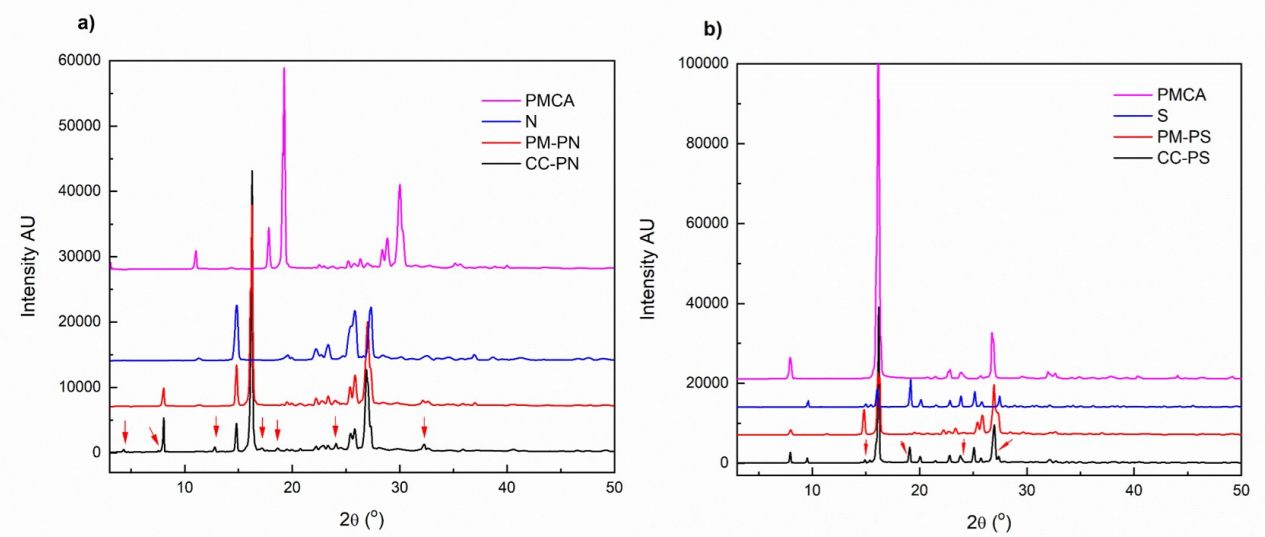


**Figure 4.** X-ray Diffraction Patterns of (a) *p*MCA (Pink Line), Nicotinamide (Blue Line), PM-PN (Red Line), and CC-PN (Black Line); and (b) *p*MCA (Pink Line), Saccharine (Blue Line), PM-PS (Red Line), and CC-PS (Black Line). Additional Peak and Reduction in Peak Intensity are Notify by the Red Arrows on CC-PN (a) and CC-PS (b), Respectively

bands at 3086 and 2958 $cm^{-1}$. The formation of cocrystals is evidenced by distinct peak shifts and band replacements in the FTIR spectra.

In the *p*MCA-nicotinamide system, noticeable shifts were observed in both the –OH/$NH_2$ and C=C stretching regions. The characteristic bands of *p*MCA at 2954, 2837, 1587.60, and 1502.75 $cm^{-1}$ and those of nicotinamide at 3358, 3150, 1612.59, and 1482.41 $cm^{-1}$ shifted to new positions at 3360, 3165, 2967, 1599.96, and 1479.64 $cm^{-1}$ in the cocrystal spectrum. These changes indicate the formation of intermolecular hydrogen bonds between the –OH group of *p*MCA and the $NH_2$ group of nicotinamide. Additionally, the appearance of a new band at 1627 $cm^{-1}$ suggests further interaction between the C=O group of nicotinamide and the –OH group of *p*MCA, which imply the the formation of a new supramolecular structure in the *p*MCA-nicotinamide cocrystal. Changes were also observed in the C–N stretching region of nicotinamide, further supporting intermolecular interactions.

In the *p*MCA-saccharin system, the O–H stretching bands of *p*MCA at 3024.51, 2931.29, 2837, and 2495.62 $cm^{-1}$ disappeared or shifted in both the physical mixture and the cocrystal to 3086 and 2967 $cm^{-1}$, indicating hydrogen bond formation between the –OH groups of *p*MCA and saccharin. Additionally, the CCPS cocrystal exhibited new peaks corresponding to asymmetric and symmetric S=O stretching vibrations around 1456 $cm^{-1}$ compared to the parent components, suggesting hydrogen bonding between the sulfonyl group of saccharin and the –OH group of *p*MCA. Further evidence of cocrystal formation was provided by shifts in saccharin's S=O stretching bands from 1329.16 and 1173.95 $cm^{-1}$ to 1330.12 and 1178.88 $cm^{-1}$, respectively, along with a shift in the C=O stretching band of *p*MCA from 1703.32 to 1718.69 $cm^{-1}$. A slight shift in the N–H stretching vibration of saccharin from 3085.31 to 3091.30 $cm^{-1}$ was also observed, collectively confirming the presence of new intermolecular hydrogen-bonding interactions in the *p*MCA-saccharin cocrystal.

These spectral changes confirm cocrystallization of *p*MCA with both coformers through non-covalent interaction mechanisms. According to reports on aromatic cocrystals, the shifts in the C=C and C–N bands for the *p*MCA-nicotinamide cocrystal show $\pi$-$\pi$ stacking between the pyridine ring of nicotinamide and the aromatic rings of *p*MCA (Thakuria and Sarma, 2018). In contrast, the *p*MCA-saccharin cocrystal is subject by hydrogen bond, as shown by the disappearance and shifts of O–H and S=O bands and supported by changes in C=O and N–H vibrations, indicating O–H···O=S and C=O···H–N interactions. The lack of notable changes in aromatic C=C and C–H bands further suggests minimal $\pi$-$\pi$ stacking in this system. Together, these findings demonstrate that the coformer dictates the dominant interaction motif and, consequently, the supramolecular organization of the resulting cocrystals (Chadha et al., 2017).

### 3.2 Thermal Analysis

DSC thermograms were used to evaluate thermal behavior and to identify potential formation of new crystalline phases during cocrystallization (Figure 2a and 2b). Pure *p*MCA exhibited a sharp endothermic peak at 172 °C and 189 °C, corresponding to its melting point, while nicotinamide and saccharin melted at 133 °C and 227 °C, respectively. At lower temperatures (120 °C and 164 °C, respectively), the physical mixtures (PM-PN and PM-PS) displayed new endothermic peaks before the distinctive peaks of each component vanished. These changes suggest the presence of intermolecular interactions between *p*MCA and the coformers and indicate the possibility of partial

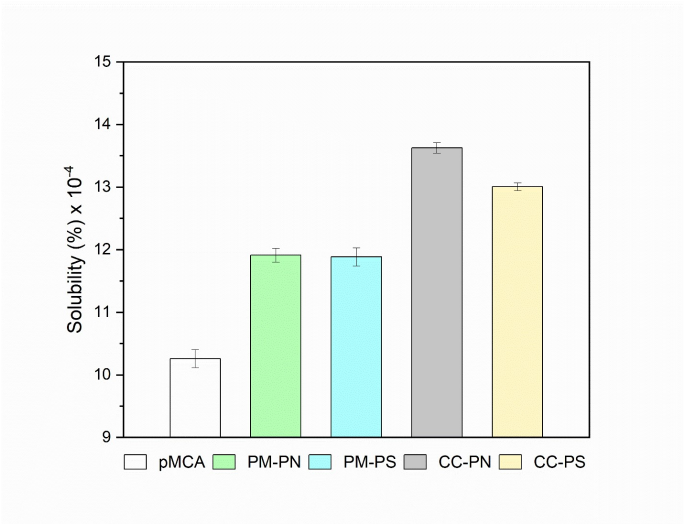


**Figure 5.** Comparison of Pure *p*MCA, Physical Mixture *p*MCA - Nicotinamide (PM-PN), Physical Mixture *p*MCA - Saccharine (PM-PS), Cocrystal *p*MCA - Nicotinamide (CC-PN), and Cocrystal *p*MCA - Saccharine (CC-PS). Data Points Represent Values ($n$=3), and Error Bars Denote Standard Deviation

cocrystal formation even at the physical mixing stage. This behavior was further supported by the cocrystals, which showed separate melting endotherms at 124.57 °C and 164.87 °C, respectively, that differed from those of their pure components.

The appearance of single, new melting peaks for both cocrystals provides strong evidence for the formation of homogeneous crystalline phases rather than simple physical mixtures, which is characteristic of true cocrystals (Kamis et al., 2020; Saganowska and Wesolowski, 2018). The lower melting temperatures of the cocrystals compared with pure *p*MCA indicate altered lattice energies and new molecular packing arrangements arising from non-covalent interactions between *p*MCA and the coformers. Notably, CC-PS exhibited a higher melting point and enthalpy of fusion (ΔHf = -451.38 J/g) than CC-PN (ΔHf = -313.77 J/g), indicating greater lattice cohesion and thermal stability for the saccharin-based cocrystal (Svärd et al., 2020). This increased stability is consistent with the formation of strong hydrogen bonds between the carboxylic acid group of *p*MCA and the sulfonyl group of saccharin, as shown by FTIR analysis. In contrast, the lower melting point and enthalpy of fusion of CC-PN suggest a less tightly packed lattice, primarily stabilized by $\pi$-$\pi$ stacking and weaker hydrogen bonding, which explains its lower thermal stability (Wicaksono et al., 2017).

### 3.3 Surface Morphology

SEM imaging at 2000× magnification was used to assess morphological changes associated with cocrystal formation, with representative micrographs shown in Figure 3a and 3b. Pure *p*MCA displayed elongated, rod-like crystals with a wood-blade appearance, consistent with anisotropic crystal growth. Nicotinamide appeared as aggregates of small elongated particles with rounded ends, while saccharin exhibited a flat, plate-like morphology. These distinct shapes served as reference baselines for evaluating the structural changes following microwave-assisted cocrystallization. A pronounced transformation was observed in CC-PN, which formed slender, well-defined prismatic columns with a compact and uniform arrangement, indicating the development of a new crystalline phase. In contrast, CC-PS showed less dramatic morphological changes, largely retaining saccharin-like plate structures, though with reduced particle size and increased particle density.

The clear differences between the cocrystals and their parent components confirm successful solid-state modification during cocrystallization (Setyawan et al., 2014). The substantial morphological restructuring observed in CC-PN reflects intermolecular interactions leading to change of molecular packing, supporting FTIR and DSC results that indicate $\pi$-$\pi$ stacking and hydrogen bonding. Conversely, the relatively modest changes in CC-PS suggest weaker interactions and limited lattice rearrangement.

Additionally, particle size analysis of the SEM images using ImageJ revealed notable changes in the particle size of the cocrystals compared to pure *p*MCA, as summarized in Figure 3. The CCPS cocrystal showed a significant reduction in particle size along with a more homogeneous particle size distribution, which is expected to enhance solubility and dissolution due to the increased surface area in contact with the aqueous medium (Huang et al., 2019). Although the CCPN cocrystal exhibited a larger apparent particle size distribution (81.61 $\mu$m), this was attributed to the aggregation of smaller primary particles that could not be individually distinguished, a phenomenon that may also contribute to improved solubility. The enhancement in kinetic solubility and dissolution of *p*MCA can be attributed not only to particle size reduction but also to modifications in crystal lattice energy and the formation of intermolecular hydrogen bonding within the cocrystal structures.

### 3.4 Crystallinity

PXRD patterns of pure *p*MCA, the coformers (nicotinamide and saccharin), their physical mixtures, and the corresponding cocrystals were recorded over a 2$\theta$ range of 1°-50°, as shown in Figure 4a and 4b. Both *p*MCA and the coformers exhibited sharp and intense diffraction peaks, confirming their crystalline nature (Kakran et al., 2011). *p*MCA showed characteristic peaks at 2$\theta$ values of 11.04°, 17.8°, 19.27°, 24.59°, 25.78°, 27.03°, 27.31°, 30.02°, 32.76°, and 40.00°. Nicotinamide and saccharin also produced distinct and well-defined peaks at their respective characteristic angles with only different intensity (Setyawan et al., 2014), which were consistent with previously reported data for these compounds (Nawatila et al., 2017; Rahman et al., 2012).

The diffractograms of the PMs displayed a simple superposition of the diffraction patterns of *p*MCA and each coformer, with no additional peaks and only minor changes in peak intensity. This indicates that physical mixing alone did not produce

new solid phases or induce structural modification of either component. In contrast, the CC-PN showed several new peaks at $2\theta$ = 4.28°, 7.92°, 12.86°, 17.19°, 18.69°, 24.07° and 32.03°, which were not present in nicotinamide or *p*MCA (red arrow, Figure 4). Strong evidence for the creation of a new crystalline lattice phase is provided by these new peaks as well as the decreased intensity of multiple parent peaks (Chadha et al., 2017). By comparison, the PXRD pattern of the CC-PS did not reveal any new diffraction peaks but showed slight shifts and reduced peak intensities relative to the parent compounds at $2\theta$ =14.91°, 19.12°, 24.06° and 27.40° (red arrow, Figure 4b). These changes suggest alterations in crystallinity or partial solid-state interaction rather than the formation of a distinct new crystalline phase. The presence of a succinate in the cocrystal structure caused the lowering of crystallinity, which affected the co-crystal lattice's regularity (Wicaksono et al., 2019).

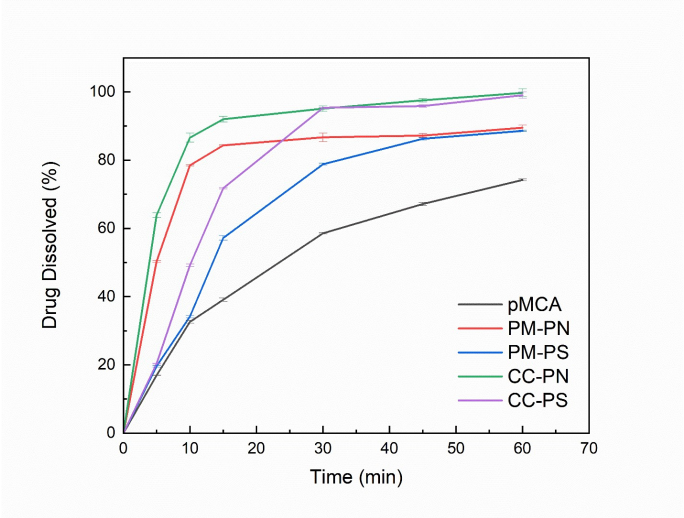


**Figure 6.** Dissolution Profiles of between Pure *p*MCA, Physical Mixture *p*MCA - Nicotinamide (PM-PN), Physical Mixture *p*MCA - Saccharine (PM-PS), Cocrystal *p*MCA - Nicotinamide (CC-PN), and Cocrystal *p*MCA - Saccharine (CC-PS) in Phosphate Buffer (pH 6.8). Data Points Represent Values ($n$=3), and Error Bars Denote Standard Deviation

### 3.5 Solubility Study

The solubility study were conducted to observed the saturated amount of *p*MCA in of phosphate buffer (pH 6.8) at 25 °C. The solubility profiles including *p*MCA, physical mixture and cocrystals formed using nicotinamide and succinate are presented in Figure 5. The results revealed a marked increase in solubility when *p*MCA was converted into both physical mixtures and cocrystals compared to pure *p*MCA. The CC-PN exhibited the highest solubility, increasing by approximately 1.29-fold relative to pure *p*MCA, whereas the CC-PS showed a 1.26-fold increase. Meanwhile, the physical mixture using nicotinamide and succinate shows similar increases by increasing *p*MCA solubility by 10%. A significant difference between the test groups was confirmed by statistical analysis using one-way ANOVA at a 95% confidence level ($\alpha$ = 0.05) ($p < 0.05$). The solubility of both physical mixes and cocrystals was considerably higher than that of pure *p*MCA, according to additional pairwise comparisons using the Post Hoc LSD test.

Nicotinamide and *p*MCA interacted through hydrogen bonds and $\pi$-$\pi$ interactions. Nicotinamide's N-pyridine and the hydroxyl group of *p*MCA generate hydrogen bonds (hydroxyl-pyridine heterosynthons). Additionally, these interactions promote the formation of a hydrogen-bonded sheet structure by linking the hydrogen-bond chains formed by nicotinamide molecules. The presence of acid-amide heterosynthons between the amide group of nicotinamide and the carboxylic acid group of *p*MCA further strengthens and organizes the crystal lattice (Setyawan et al., 2025). However, because nicotinamide is highly soluble relative to the cocrystal, it readily dissolves from the lattice when in contact with the dissolution medium, leaving void spaces within the crystal structure. This disruption weakens the intermolecular connectivity and facilitates partial structural collapse, which in turn enhances water penetration and increases the apparent solubility of the cocrystal (Zaini et al., 2020).

### 3.6 Dissolution Study

The comparative dissolution profiles between *p*MCA, physical mixture and cocrystals in both *p*MCA-nicotinamide system and *p*MCA-saccharin system is presented in Figure 6. Evaluation using the similarity factor ($f_2$) equation (Equation 1) showed that none of the dissolution profiles were similar, as all $f_2$ values were below 50, indicating distinct dissolution behaviors among the samples. Furthermore, differences in dissolution rates were assessed using the Hixson-Crowell model (Equation 2), which describes dissolution behavior when a linear relationship is obtained between the cubic root of the initial drug amount minus the cubic root of the remaining undissolved amount (Y-axis) and time (X-axis) (Johnson et al., 2018). All samples showed a significant increase in dissolution within the first 15 minutes. The early dissolution rate was quantified by calculating the slope of the linear regression of $M_0^{1/3}$ - $M^{1/3}$ versus time (5-15 min) presented in Table 1. where higher slope values indicate faster dissolution. Statistical analysis using one-way ANOVA ($\alpha$ = 0.05) revealed significant differences among the samples, and subsequent Post Hoc LSD testing identified specific pairwise differences.

The analysis indicates that the percentage of drug dissolved from both the physical mixtures and cocrystals increased compared to pure *p*MCA, which is consistent with the calculated dissolution rates (slopes). Pure *p*MCA dissolved only 58% within 30 minutes, whereas both cocrystals achieved approximately 95% dissolution within the same time period. Among the physical mixtures, PS-PN exhibited a higher dissolution percentage than PS-PS, reaching 86% and 78%, respectively, at 30 minutes. The dissolution profiles further demonstrate that both cocrystals provided faster and more complete drug release than

their corresponding physical mixtures. Specifically, CC-PN showed a 3.67-fold increase in dissolution rate compared to pure *p*MCA, while CC-PS exhibited a 3.55-fold increase. In contrast, the physical mixtures showed lower enhancements, with PS-PN and PS-PS displaying 3.02-fold and 1.5-fold increases in dissolution rate, respectively. These findings are consistent with previously reported studies involving nicotinamide and saccharin as coformers, which have demonstrated similar enhancements in dissolution behavior. Cocrystals using nicotinamide as a coformer have shown increases in dissolution efficiency of 3.61 -fold (Setyawan et al., 2025), 2.50 -fold (Chadha et al., 2017), 5.50 -fold (Xiao et al., 2022),13.50 -fold (Wichianphong and Charoenchaitrakool, 2018), and 3.44 -fold (Panzade and Shendarkar, 2019) across various active pharmaceutical ingredients. Similarly, saccharin-based cocrystals have been reported to enhance dissolution by up to 4.8-fold (Prashanth et al., 2022) and 3.6-fold (Jung et al., 2010).

The enhanced dissolution of the cocrystals can be explained by structural and thermodynamic modifications induced by coformer interactions. However, it is anticipated that cocrystals would enhance its dissolution performance due to a high Gibbs free energy and since less energy is required to withdraw molecules from the disordered solid compared with a crystalline material (Prashanth et al., 2022). Cocrystallization disrupts the *p*MCA lattice, reducing crystallinity and improving wettability, which facilitates faster solvent penetration and dissolution (Huang et al., 2019; Li and Matzger, 2017; Xia et al., 2022). The *p*MCA-nicotinamide cocrystal showed greater solubility and dissolution than the *p*MCA-saccharin system, attributed to higher intrinsic solubility of nicotinamide (≈ 500 mg/mL at 25 °C) compared to saccharin (≈ 4 mg/mL at 25 °C) and weaker lattice packing, which promotes easier lattice disruption. In contrast, the stronger hydrogen bonding in the *p*MCA-saccharin cocrystal produced greater stability but slower dissolution. This behavior aligns with the "spring-parachute" mechanism (Sathisaran and Dalvi, 2018), where rapid lattice breakdown initially increases solubility ("spring effect"), followed by coformer-mediated stabilization of the supersaturated state ("parachute effect") (Bavishi and Borkhataria, 2016). Together, these factors explain the superior dissolution performance of the *p*MCA-nicotinamide cocrystal.

Collectively, FTIR, DSC, SEM, and PXRD analyses confirm the successful formation of cocrystals between *p*MCA and both coformers, albeit through distinct interaction mechanisms. Nicotinamide predominantly participates in $\pi$-$\pi$ stacking interactions accompanied by weaker hydrogen bonding, resulting in a cocrystal with enhanced solubility and faster dissolution despite a broader apparent particle size distribution, which is likely attributable to particle aggregation (Figure 3). In contrast, saccharin forms stronger and more extensive hydrogen-bonded networks, leading to higher lattice stability and melting points but comparatively slower dissolution, even though a smaller and more uniform particle size distribution was observed (Figure 3). These findings underscore the critical role of coformer selection in tailoring the physicochemical properties of cocrystals, with CC-PN demonstrating superior solubility and dissolution performance, while CC-PS offering greater thermal and structural stability. The appearance of distinct new peaks absent in the physical mixtures, together with corroborating PXRD patterns and observable changes in crystal morphology, further confirms the formation of new crystalline phases. Ultimately, understanding the trade-off between solubility enhancement and stability is essential for rational cocrystal design in pharmaceutical development. Notably, the microwave-assisted preparation method proved to be a promising approach, yielding high cocrystal production efficiency and excellent reproducibility.

## 4. CONCLUSIONS

This study confirmed the successful formation of *p*MCA cocrystals with nicotinamide and saccharin, as evidenced by FTIR, DSC, SEM, and PXRD analyses. Both systems exhibited distinct interaction mechanisms that influenced their physicochemical properties. The CC-PN was stabilized by $\pi$-$\pi$ stacking and weak hydrogen bonds, lead to in lower lattice energy, smaller particle size, and significantly increased solubility and dissolution. In contrast, the CC-PS formed strong O–H···O=S hydrogen bonds, leading to higher thermal stability and greater lattice cohesion but slower dissolution behavior. These findings demonstrate that coformer selection plays a critical role in tuning the balance between solubility enhancement and structural stability. Overall, nicotinamide was identified as the more effective coformer for improving the solubility performance of *p*MCA, while saccharin favored thermal and crystalline stability, underscoring the importance of rational coformer design in pharmaceutical cocrystal development.

## 5. ACKNOWLEDGEMENT

The authors express gratitude to Universitas Airlangga for supporting this research through the Airlangga Research Fund (ARF) with contract number 1146/UN3.1.5/LT/2018.

## REFERENCES

Abdullah, A., M. Mutmainnah, and E. R. Wikantyasning (2022). Cocrystals of Cefixime with Nicotinamide: Improved Solubility, Dissolution, and Permeability. *Indonesian Journal of Pharmacy*, **33**(3); 394–400

Adisakwattana, S., S. Roengsamran, W. H. Hsu, and S. Yibchok-Anun (2005). Mechanisms of Antihyperglycemic Effect of p-Methoxycinnamic Acid in Normal and Streptozotocin-Induced Diabetic Rats. *Life Sciences*, **78**(4); 406–412

Ahammad, T., M. Begum, A. F. M. Towheedur Rahman, M. Hasan, S. R. Paul, S. Eamen, M. I. Hussain, M. H. Ali, M. A. Islam, M. M. Rahman, and M. Rashid (2015). Formulation and *In Vitro* Release Pattern Study of Gliclazide Matrix Tablet. *Pharmacology & Pharmacy*, **6**(3); 125–131

Ahmad, S., R. Jaiswal, R. Yadav, and S. Verma (2024). Recent

 

Advances in Green Chemistry Approaches for Pharmaceutical Synthesis. *Sustainable Chemistry One World*, **4**; 100029

Basavoju, S., D. Boström, and S. P. Velaga (2008). Indomethacin-Saccharin Cocrystal: Design, Synthesis and Preliminary Pharmaceutical Characterization. *Pharmaceutical Research*, **25**(3); 530–541

Bavishi, D. D. and C. H. Borkhataria (2016). Spring and Parachute: How Cocrystals Enhance Solubility. In *Progress in Crystal Growth and Characterization of Materials*, volume 62. Elsevier Ltd., pages 1–8

Chadha, R., D. Rani, and P. Goyal (2017). Supramolecular Cocrystals of Gliclazide: Synthesis, Characterization and Evaluation. *Pharmaceutical Research*, **34**(3); 552–563

Chaves Júnior, J. V., J. A. B. dos Santos, T. B. Lins, R. S. de Araújo Batista, S. A. de Lima Neto, A. de Santana Oliveira, F. H. A. Nogueira, A. P. B. Gomes, D. P. de Sousa, F. S. de Souza, and C. F. S. Aragão (2020). A New Ferulic Acid-Nicotinamide Cocrystal with Improved Solubility and Dissolution Performance. *Journal of Pharmaceutical Sciences*, **109**(3); 1330–1337

Dias, J. L., E. A. Rebelatto, D. Hotza, A. J. Bortoluzzi, M. Lanza, and S. R. S. Ferreira (2022). Production of Quercetin-Nicotinamide Cocrystals by Gas Antisolvent (GAS) Process. *Journal of Supercritical Fluids*, **188**; 105670

Diaz, D. A., S. T. Colgan, C. S. Langer, N. T. Bandi, M. D. Likar, and L. Van Alstine (2016). Dissolution Similarity Requirements: How Similar or Dissimilar Are the Global Regulatory Expectations? *AAPS Journal*, **18**(1); 15–22

Ekowati, J. and N. W. Diyah (2013). Antinociceptive *In Silico* Cyclooxygenase of *p*-Methoxycinnamic Acid. *Berkala Ilmiah Kimia Farmasi*, **2**(1); 33–40

Gillespie, P. M. (2005). Microwave Chemistry: An Approach to the Assessment of Chemical Reaction Hazards. In *Institution of Chemical Engineers Symposium Series*, volume 150. Institution of Chemical Engineers, pages 533–543

Huang, Y., G. Kuminek, L. Roy, K. L. Cavanagh, Q. Yin, and N. Rodríguez-Hornedo (2019). Cocrystal Solubility Advantage Diagrams as a Means to Control Dissolution, Supersaturation, and Precipitation. *Molecular Pharmaceutics*, **16**(9); 3887–3895

Johnson, P., V. Krishnan, C. Loganathan, K. Govindhan, V. Raji, P. Sakayanathan, S. Vijayan, P. Sathishkumar, and T. Palvannan (2018). Rapid Biosynthesis of *Bauhinia variegata* Flower Extract-Mediated Silver Nanoparticles: An Effective Antioxidant Scavenger and $\alpha$-Amylase Inhibitor. *Artificial Cells, Nanomedicine and Biotechnology*, **46**(7); 1488–1494

Jung, M. S., J. S. Kim, M. S. Kim, A. Alhalaweh, W. Cho, S. J. Hwang, and S. P. Velaga (2010). Bioavailability of Indomethacin–Saccharin Cocrystals. *Journal of Pharmacy and Pharmacology*, **62**(11); 1560–1568

Kakran, M., N. G. Sahoo, and L. Li (2011). Dissolution Enhancement of Quercetin Through Nanofabrication, Complexation, and Solid Dispersion. *Colloids and Surfaces B: Biointerfaces*, **88**(1); 121–130

Kamis, M. N. A. A., H. M. Zaki, N. Anuar, and M. N. Jalil (2020). Synthesis, Characterization and Morphological Study of Nicotinamide and *p*-Coumaric Acid Cocrystal. *Indonesian Journal of Chemistry*, **20**(3); 661–679

Karagianni, A., M. Malamatari, and K. Kachrimanis (2018). Pharmaceutical Cocrystals: New Solid Phase Modification Approaches for the Formulation of APIs. *Pharmaceutics*, **10**(1); 18

Li, Z. and A. J. Matzger (2017). Influence of Coformer Stoichiometric Ratio on Pharmaceutical Cocrystal Dissolution: Three Cocrystals of Carbamazepine/*p*-Aminobenzoic Acid. *Molecular Pharmaceutics*, **14**(1); 139–148

Miroshnyk, I., S. Mirza, and N. Sandler (2009). Pharmaceutical Co-Crystals: An Opportunity for Drug Product Enhancement. *Expert Opinion on Drug Delivery*, **6**(4); 333–341

Nawatila, R., W. Agnes Nuniek, S. Siswodihardjo, and D. Setyawan (2017). Preparation of Acyclovir-Nicotinamide Cocrystal by Solvent Evaporation Technique with Variation of Solvent. *Asian Journal of Pharmaceutical and Clinical Research*, **10**(3); 283–287

Nyamba, I., C. B. Sombie, M. Yabre, H. Zime-Diawara, J. Yameogo, S. Ouedraogo, A. Lechanteur, R. Semde, and B. Evrard (2024). Pharmaceutical Approaches for Enhancing Solubility and Oral Bioavailability of Poorly Soluble Drugs. *European Journal of Pharmaceutics and Biopharmaceutics*, **204**; 114513

Pagire, S., S. Korde, R. Ambardekar, S. Deshmukh, R. C. Dash, R. Dhumal, and A. Paradkar (2013). Microwave Assisted Synthesis of Caffeine/Maleic Acid Co-Crystals: The Role of the Dielectric and Physicochemical Properties of the Solvent. *CrystEngComm*, **15**(18); 3705–3710

Palanisamy, M. and J. Khanam (2011). Solid Dispersion of Prednisolone: Solid State Characterization and Improvement of Dissolution Profile. *Drug Development and Industrial Pharmacy*, **37**(4); 373–386

Panzade, P. and G. Shendarkar (2019). Superior Solubility and Dissolution of Zaltoprofen via Pharmaceutical Cocrystals. *Turkish Journal of Pharmaceutical Sciences*, **16**(3); 310–316

Prashanth, J., K. V. Drozd, G. L. Perlovich, S. Balasubramanian, and A. Surov (2022). Cocrystal and Coamorphous Solid Forms of Enzalutamide with Saccharin: Structural Characterization and Dissolution Studies. *Crystal Growth & Design*, **22**(11); 6703–6716

Puspita, O. E., M. I. Sulistyowaty, R. Salam, and D. Setyawan (2025). Microwave-Assisted Synthesis: A Green Chemistry Approach for Drug Cocrystals Synthesis. In *Science and Technology Indonesia*, volume 10. Magister Program of Material Sciences, Graduate School of Sriwijaya University, pages 1130–1147

Qiao, N., M. Li, W. Schlindwein, N. Malek, A. Davies, and G. Trappitt (2011). Pharmaceutical Cocrystals: An Overview. *International Journal of Pharmaceutics*, **419**(1–2); 1–11

Rahman, Z., R. Samy, V. A. Sayeed, and M. A. Khan (2012). Physicochemical and Mechanical Properties of Car-

 

bamazepine Cocrystals with Saccharin. *Pharmaceutical Development and Technology*, **17**(4); 457–465

Saganowska, P. and M. Wesolowski (2018). DSC as a Screening Tool for Rapid Co-Crystal Detection in Binary Mixtures of Benzodiazepines with Co-Formers. *Journal of Thermal Analysis and Calorimetry*, **133**(1); 785–795

Sathisaran, I. and S. V. Dalvi (2018). Engineering Cocrystals of Poorly Water-Soluble Drugs to Enhance Dissolution in Aqueous Medium. *Pharmaceutics*, **10**(3); 108

Savjani, K. T., A. K. Gajjar, and J. K. Savjani (2012). Drug Solubility: Importance and Enhancement Techniques. *International Scholarly Research Notices*, **2012**(1); 195727

Setyawan, D., A. Paramanandana, V. E. Erfadrin, R. Sari, and P. Diajeng Putri (2020). Compression Force Effect on Characteristics of Loratadine–Succinic Acid Cocrystal Prepared by Slurry Method. *Journal of Research in Pharmacy*, **24**(3); 410–415

Setyawan, D., S. A. Permata, A. Zainul, and M. L. A. Dwi Lestari (2018). Improvement *In Vitro* Dissolution Rate of Quercetin Using Cocrystallization of Quercetin–Malonic Acid. *Indonesian Journal of Chemistry*, **18**(3); 531–536

Setyawan, D., R. Sari, H. Yusuf, and R. Primaharinastiti (2014). Preparation and Characterization of Artesunate–Nicotinamide Cocrystal by Solvent Evaporation and Slurry Method. *Asian Journal of Pharmaceutical and Clinical Research*, **7**(Suppl. 1); 62–65

Setyawan, D., Y. Soraya, J. Ekowati, A. N. Winantari, K. C. Rani, F. A. T. Kanzaffa, and F. E. Pujiono (2025). Enhancing *In Vitro* Dissolution of Ferulic Acid Through Co-Crystal Formation Using Malonic Acid and Nicotinamide Co-Formers. *Science and Technology Indonesia*, **10**(4); 1255–1269

Sinko, P. J. and Y. Singh (2011). *Martin's Physical Pharmacy and Pharmaceutical Sciences*. Lippincott Williams & Wilkins, 6th edition

Subositi, D., N. Kurnianingrum, R. Mujahid, and Y. Widiyastuti (2020). *Kaempferia galanga* L.: A Medicinal Plant Used by Indonesian Ethnic Groups. *Biodiversitas*, **42**(1); 45–52

Sulistyowaty, M. I., S. Fitri, N. Yuliati, T. Amrillah, C. A. C. Abdullah, and D. Setyawan (2024). Solubility and Dissolution Improvement of Paramethoxycinnamic Acid (PMCA) Induced by Cocrystal Formation Using Caffeine as a Co-former. *Sains Malaysiana*, **53**(10); 3445–3454

Svärd, M., D. Ahuja, and Å. C. Rasmuson (2020). Calorimetric Determination of Cocrystal Thermodynamic Stability: Sulfamethazine–Salicylic Acid Case Study. *Crystal Growth & Design*, **20**(7); 4243–4251

Tambosi, G., P. F. Coelho, S. Luciano, I. C. S. Lenschow, M. Zétola, H. K. Stulzer, and B. R. Pezzini (2018). Challenges to Improve the Biopharmaceutical Properties of Poorly Water-Soluble Drugs and the Application of the Solid Dispersion Technology. *Matéria (Rio de Janeiro)*, **23**(4); e12224

Thakuria, R. and B. Sarma (2018). Drug-Drug and Drug-Nutraceutical Cocrystal/Salt As Alternative Medicine for Combination Therapy: A Crystal Engineering Approach. *Crystals*, **8**(2); 101

Wicaksono, Y., D. Setyawan, and Siswandono (2017). Formation of Ketoprofen–Malonic Acid Cocrystal by Solvent Evaporation Method. *Indonesian Journal of Chemistry*, **17**(2); 161–166

Wicaksono, Y., D. Setyawan, S. Siswandono, and T. A. Siswoyo (2019). Preparation and Characterization of a Novel Cocrystal of Atorvastatin Calcium with Succinic Acid Coformer. *Indonesian Journal of Chemistry*, **19**(3); 660–667

Wichianphong, N. and M. Charoenchaitrakool (2018). Statistical Optimization for Production of Mefenamic Acid–Nicotinamide Cocrystals Using Gas Anti-Solvent (GAS) Process. *Journal of Industrial and Engineering Chemistry*, **62**; 375–382

Xia, M. Y., B. Q. Zhu, J. R. Wang, Z. E. Yang, and X. F. Mei (2022). Superior Dissolution Behavior and Bioavailability of Pharmaceutical Cocrystals and Recent Regulatory Issues. *ACS Medicinal Chemistry Letters*, **13**(1); 29–37

Xiao, Y., T. Jin, X. Geng, and X. Zhu (2022). Azilsartan–Nicotinamide Cocrystal: Preparation, Characterization and *In Vitro*/*In Vivo* Evaluation. *European Journal of Pharmaceutical Sciences*, **176**; 106241

Zaini, E., Afriyani, L. Fitriani, F. Ismed, A. Horikawa, and H. Uekusa (2020). Improved Solubility and Dissolution Rates in Novel Multicomponent Crystals of Piperine with Succinic Acid. *Scientia Pharmaceutica*, **88**(2); 21

 